

# 1 Retrieval of ammonia from ground-based FTIR solar spectra

2  
3 E. Dammers<sup>1</sup>, C. Vigouroux<sup>2</sup>, M. Palm<sup>3</sup>, E. Mahieu<sup>4</sup>, T. Warneke<sup>3</sup>, D. Smale<sup>5</sup>, B.Langerock<sup>2</sup>, B. Franco<sup>4</sup>, M. Van  
4 Damme<sup>1,6</sup>, M. Schaap<sup>7</sup>, J. Notholt<sup>3</sup> and J.W. Erisman<sup>1,8</sup>

5 1. Cluster Earth and Climate, Department of Earth Sciences, Vrije Universiteit Amsterdam, Amsterdam, the  
6 Netherlands

7 2. Belgian Institute for Space Aeronomy, Brussels, Belgium

8 3. Institut für Umweltphysik, University of Bremen, Bremen, Germany

9 4. Institute of Astrophysics and Geophysics, University of Liege, Belgium

10 5. National Institute of Water and Atmosphere, Lauder, New Zealand

11 6. Spectroscopie de l'Atmosphère, Service de Chimie Quantique et Photophysique, Université Libre de Bruxelles,  
12 Brussels, Belgium

13 7. TNO Built Environment and Geosciences, Department of Air Quality and Climate, Utrecht, the Netherlands

14 8. Louis Bolk Institute, Driebergen, the Netherlands

15  
16 **Abstract** We present a retrieval method for ammonia (NH<sub>3</sub>) total columns from ground-based Fourier  
17 Transform InfraRed (FTIR) observations. Observations from Bremen (53.10N, 8.85E), Lauder (45.04S,  
18 169.68E), Reunion (20.9S, 55.50E) and Jungfraujoch (46.55N, 7.98E) were used to illustrate the capabilities of  
19 the method. NH<sub>3</sub> mean total columns ranging three orders of magnitude were obtained with higher values at  
20 Bremen (mean of 13.47e15 molecules cm<sup>-2</sup>) to the lower values at Jungfraujoch (mean of 0.18e15 molecules  
21 cm<sup>-2</sup>). In conditions with high surface concentrations of ammonia, as in Bremen, it is possible to retrieve  
22 information on the vertical gradient as two layers can be discriminated. The retrieval there is most sensitive to  
23 ammonia in the planetary boundary layer, where the trace gas concentration is highest. For conditions with low  
24 concentrations only the total column can be retrieved. Combining the systematic and random errors we have a  
25 mean total error of 26% for all spectra measured at Bremen (Number of spectra (N) =554), 30% for all spectra  
26 from Lauder (N=2412), 25% for spectra from Reunion (N=1262) and 34% for spectra measured at Jungfraujoch  
27 (N=2702). The error is dominated by the systematic uncertainties in the spectroscopy parameters. Station  
28 specific seasonal cycles were found to be consistent with known seasonal cycles of the dominant ammonia  
29 sources in the station surroundings. The developed retrieval methodology from FTIR-instruments provides a  
30 new way to obtain highly time-resolved measurements of ammonia burdens. FTIR-NH<sub>3</sub> observations will be  
31 useful for understanding the dynamics of ammonia concentrations in the atmosphere and for satellite and model  
32 validation. It will also provide additional information to constrain the global ammonia budget.

33

34

## 35 1. Introduction

36 Nitrogen emissions in the form of ammonia ( $\text{NH}_3$ ), which largely derive from agriculture, have been associated  
37 with acidification and eutrophication of soils and surface waters (Krupa, 2003; Vitousek et al., 1997), which may  
38 reduce biodiversity in vulnerable ecosystems (Bobbink et al., 1998, 2010). Ammonia also reacts with nitric acid  
39 and sulphuric acid to form ammonium salts, which account for a large fraction of particulate matter concentrations  
40 (Schaap et al., 2004). Particulate matter is a major contributor to smog and is related to negative health impacts  
41 (Pope et al., 2009). Moreover ammonium salts play an important role in the radiance balance of the Earth, thus  
42 having an impact on climate change (Charlson et al., 1991, Erisman et al., 2007). It was shown that reduced  
43 nitrogen also plays a role in the fixation of carbon dioxide ( $\text{CO}_2$ ) (Reay et al., 2008). Human activities have  
44 increased the global emissions of reactive nitrogen (Nr) to the atmosphere (Holland et al., 1999). Current global  
45 Nr emissions have been estimated to be almost four times larger compared to pre-industrial levels (Fowler et al.,  
46 2013) with  $\text{NH}_3$  emissions amounting to 49.3Tg in 2008 (EDGAR-Emission Database for Global Atmospheric  
47 Research, 2011). Consequently this has led to large increases in atmospheric nitrogen deposition (Rodhe et al.,  
48 2002; Dentener et al., 2006). Biomass burning was found to account for 11% of the global emission budget of  
49  $\text{NH}_3$  (Bouwman et al., 1997). While the agricultural emissions dominate in the Northern Hemisphere, biomass  
50 burning is one of the main sources of the  $\text{NH}_3$  concentrations in the Southern Hemisphere.

51 Despite its central role in many environmental threats, little is known about the ammonia budget and its  
52 distribution across the globe. Uncertainties in global and regional emission rates are large with errors of more than  
53 50% (Erisman et al., 2007; Sutton et al., 2013). Ammonia concentrations have a large variability in time and  
54 space, a short lifetime in the order of hours, and the lack of globally distributed observations hamper our  
55 understanding. Surface observations are available, but these are not homogeneously distributed over the globe with  
56 most observation sites located in the Northern Hemisphere. Most sites provide data with a poor temporal resolution  
57 (e.g. many observation networks use passive samplers with a sampling time of 2 or 4 weeks (Thijsse et al., 1998;  
58 Puchalski et al., 2011)) whereas emission and deposition dynamics affect concentrations on the scale of hours to  
59 days. Systems with higher sampling frequency such as the AMANDA, MARGA and (denuder) filter packs are  
60 available, but the number of measurement networks using these instruments is limited as they are often costly to  
61 operate (Erisman et al., 2001; Thomas et al., 2009; Mount et al., 2002; Hansen et al., 2003). Moreover, measuring  
62  $\text{NH}_3$  is challenging and existing in-situ measurement techniques are often prone to sampling artefacts (Bobruzki  
63 et al., 2010). Recent advances in open path remote sensing techniques, like (mini-) DOAS systems and open path  
64 Quantum Cascaded Laser instruments show large potential to overcome part of these sampling issues (Volten et  
65 al., 2012; Miller et al., 2014), but are still in the development stage and not widely applied yet. Another aspect is  
66 the lack of vertical information, as most instruments only measure surface concentrations (Erisman et al., 1998,  
67 2007; Van Damme et al. 2014c). Some recent airborne measurements have been made (Nowak et al., 2007, 2010;  
68 Leen et al., 2013), but only during dedicated campaigns with limited temporal and spatial coverage. In short, it is  
69 very difficult to obtain detailed knowledge on the global ammonia budget using currently available field  
70 observations.

71 Remote sensing products from atmospheric satellite sounders such as the Infrared Atmospheric Sounding  
72 Interferometer (IASI), the Tropospheric Emission Spectrometer (TES) and the Cross-track Infrared Sounder

73 (CrIS) (Van Damme et al., 2014a; Shephard et al., 2011; 2015a) have become available and show good promise  
74 to improve NH<sub>3</sub> concentration monitoring (Van Damme et al. 2014b; Luo et al., 2015; Whitburn et al. 2015).  
75 However, these data sets are constrained by the overpass time of the satellite and the atmospheric conditions  
76 (cloud coverage, thermal contrast, etc.). Moreover, the uncertainties associated to the data are relatively large,  
77 which calls for a detailed evaluation of the data. A recent study (Van Damme et al., 2014c) showed a number of  
78 challenges related to the validation. First, reliable hourly in-situ data is sparse. Second, when not using optimal  
79 estimation satellite product as is the case for the IASI- NH<sub>3</sub> retrieval, one has to assume a vertical profile to link  
80 surface concentrations to a column value. Third, the ground-based observations are often influenced by local  
81 sources, whereas satellite observations have a footprint of the order of tens on kilometres. A recent study by  
82 Shephard et al (2015b) shows the potential of an instrument that can be used for profile comparisons. In the study  
83 instruments on an aircraft were used measure a vertical profile of NH<sub>3</sub> which were used as a validation tool for  
84 the NH<sub>3</sub>-profile observations of TES. Hence, a measurement methodology that would provide columnar and  
85 vertical profiles of ammonia concentrations at a high temporal resolution would be highly beneficial for evaluating  
86 the merits of the novel satellite products. Fourier Transform infrared spectrometry (FTIR) provides this  
87 methodology. Atmospheric sounders have a long history for validation of satellite products. FTIR observations  
88 are already commonly used for the validation of satellite products of among others, carbon monoxide (CO),  
89 methane (CH<sub>4</sub>) and nitrous oxide (N<sub>2</sub>O) (Wood et al., 2002; Griesfeller et al., 2006; Dils et al., 2006;  
90 Kerzenmacher et al., 2012).

91 FTIR spectrometry is a well-established remote sensing technique for the observation of atmospheric trace gases  
92 (Rao and Weber, 1992). FTIR has so far been used to estimate ammonia emissions from fires (Yokelson et al.,  
93 1997, 2007, Paton-Walsh et al., 2005)), but only on a campaign basis, not long-term monitoring. There are several  
94 monitoring stations with FTIR instruments operated on a regular basis, providing long-term time series for a suite  
95 of key tropospheric and stratospheric species, including Carbon Dioxide (CO<sub>2</sub>), Carbon Monoxide (CO) and  
96 Ozone (O<sub>3</sub>). So far nobody has systematically analysed the FTIR measurements for NH<sub>3</sub>. We have developed a  
97 NH<sub>3</sub> retrieval strategies for four Network for detection of Atmospheric Composition Change (NDACC) FTIR  
98 stations, spanning very different concentration conditions (polluted and remote sites), in order to obtain time-  
99 series of NH<sub>3</sub> total columns and show its value for describing temporal variations.

100 First we present the measurement sites and the retrieval strategies in section 2. We describe the characteristics of  
101 the retrieval in section 3.1.1 and the uncertainty budget in section 3.1.2. Section 3.2 constitutes of an interpretation  
102 of the results in combination with a comparison with existing datasets of CO total columns and temperature to  
103 distinguish between emission sources. We summarize the results in section 4.

104

## 105 **2. Measurement sites and retrieval strategies**

106

### 107 **2.1 Sites description**

108

109 Ground-based FTIR instruments measure the solar absorption spectra under cloud-free conditions by using a  
110 Fourier Transform Spectrometer. These spectra can be analysed by using a line by line model (Pougetchev et al.,

111 1995; Hase et al., 2004, 2006), which models the spectroscopic absorption lines by using known parameters  
112 from a spectroscopic database (e.g. HITRAN, Rothman et al., 2013) in combination with the radiative state of  
113 the atmosphere, and an optimal estimation inversion scheme (Rodgers, 2000). Information on vertical  
114 concentration profiles can be retrieved using the pressure broadening of the absorption lines. For the NDACC  
115 network the spectral region measured is the near- to mid-infrared domain (740 to 4250  $\text{cm}^{-1}$ , i.e. 13.5 to 2.4  $\mu\text{m}$ )  
116 with a HgCdTe or InSb cooled detector (Zander et al., 2008) and a suite of optical filters are used to optimize  
117 the signal-to-noise ratio in the complementary spectral regions. Instruments in the network are routinely checked  
118 and characterized using laboratory measurements of HBr lines and the linefit software (Hase et al., 1999) to  
119 assess the instrument line shape, alignment and measurement noise levels. Four NDACC stations are used in our  
120 study, two in each hemisphere:

121 - The site of Bremen (53.10N, 8.85E) is especially suitable to measure variations in ammonia concentrations  
122 as the surrounding state, Lower Saxony, which is a region with intensive agricultural activities with high and  
123 temporal variable emissions (Dämmgen et al., 2005). In short, the ammonia total columns (molecules  $\text{cm}^{-2}$ )  
124 at Bremen are expected to reach high values compared to background stations. The Universität Bremen  
125 operates a Bruker 125HR spectrometer and a solar tracker by Bruker GmbH, directly on the university  
126 campus.

127

128 - The Jungfraujoch station (46.55N, 7.98E) is a high altitude station (3580 m.a.s.l.) located in Switzerland  
129 (Zander et al., 2008). There are no large emissions sources surrounding the station itself as it is mostly located  
130 in the free troposphere. At Jungfraujoch, a Bruker 120HR instrument is in operation since the early 1990s.  
131 For the current study, specific for the Jungfraujoch site, we used a subset of spectra recorded during the 2004-  
132 2013 time period with apparent solar zenith angles (SZA) between 70 and 85° to increase the capability to  
133 retrieve the very low ammonia concentrations.

134

135 - The Lauder (45.04S, 169.68E) National Institute of Water and Atmospheric Research (NIWA) atmospheric  
136 research station in Central Otago, New Zealand at an altitude of 370 (m.a.s.l.). Long-term operations started  
137 in 1991 with a Bruker 120M (Griffith et al., 2003). This instrument was replaced with a Bruker 120HR in  
138 October 2001. Ammonia emissions in the surrounding valley are mostly due to livestock grazing on the  
139 pastures and a by-product of seasonal fertilizer application. In recent years there has been an increase in cattle  
140 grazing and crop cultivation (EDGAR-Emission Database for Global Atmospheric Research, 2011).

141

142 - Reunion Island (20.9S, 55.50E) is located in the Indian Ocean to the east of Madagascar. The station is located  
143 at the University campus of St.-Denis on the north side of the island. Agricultural activities are mostly related  
144 to sugar cane production. The island is prone to some local biomass burning and wild fire events, which are  
145 known to emit ammonia. It is also very close to Madagascar, a region with frequent and intense biomass  
146 burning events, and it has been found using backward trajectory that the emissions in Madagascar can be  
147 transported to Reunion Island within one day (Vigouroux et al., 2009). The measurements used in this study  
148 are performed with a Bruker 120M spectrometer. Details on the measurements can be found in Senten et al.  
149 (2008) and Vigouroux et al. (2012).

150

151 These stations are expected to provide significant differences in variability and levels of ammonia, making them  
152 suitable to demonstrate the strength of our retrieval scheme for application across the whole network. A summary  
153 of the station descriptions is given in Table 1. CO columns were obtained from the NDACC database to be used  
154 for comparison in section 3.

155

## 156 **2.2 NH<sub>3</sub> Retrieval Strategies**

157

158 The ammonia absorption lines from its  $\nu_2$  vibrational band can be observed in the 700-1350  $\text{cm}^{-1}$  wavenumber  
159 range, which are also used in the retrieval of satellite products of ammonia (e.g. Clarisse et al., 2009, Van Damme  
160 et al., 2014a). In this spectral range the FTIR spectra can be measured using a potassium bromide (KBr) beam-  
161 splitter in combination with a mercury cadmium telluride (MCT) nitrogen cooled detector (Zander et al., 2008).  
162 The retrieval scheme of trace gas concentrations from FTIR spectra is built on the use of a set of spectral micro  
163 windows containing absorption lines of the targeted species, with minimum interference by other atmospheric  
164 species or solar lines. Two slightly different set of spectral micro-windows were used at the four stations, but they  
165 both use the same main NH<sub>3</sub> absorption lines. The target and interfering species are summarized in Table 2, with  
166 the profile retrieved species indicated in bold. To properly estimate ammonia, interfering species like O<sub>3</sub> and water  
167 vapour (H<sub>2</sub>O) that overlap NH<sub>3</sub> lines in the  $\nu_2$  vibrational band have to be accounted for. Two micro windows  
168 were chosen that contain as little interfering species as possible. In both sets, the first micro window (MW1)  
169 covers the NH<sub>3</sub> absorption line at 930.75  $\text{cm}^{-1}$ . At Bremen/Lauder, the choice was to use only isolated NH<sub>3</sub>  
170 absorption features to avoid possible problems due to line mixing, therefore the spectral window MW1 is only 1  
171  $\text{cm}^{-1}$  wide [930.32-931.32, MW1]. Figure 1 shows an example of a synthetic spectrum calculated to fit a  
172 observation that was measured with the 125HR in Bremen on the 19th of April 2010 at 09:59 (UTC) (Solar Zenith  
173 Angle of 45 degrees). The NH<sub>3</sub> concentrations on this day were slightly higher than average resulting in slightly  
174 stronger NH<sub>3</sub> absorption features in the spectra. The top two figures show the absorption contributions of the  
175 absorbing species in both micro windows. The bottom two panels show an enlarged version of the figure to  
176 distinguish the interfering species with smaller absorption features. At Reunion Island/Jungfrauoch, MW1 was  
177 extended [929.4-931.4, MW1] to cover another NH<sub>3</sub> line at 929.9  $\text{cm}^{-1}$ . This improved the retrieval for Reunion  
178 Island because at this location the NH<sub>3</sub> concentration levels are much lower than at Bremen and the water vapour  
179 concentrations are much higher. In this high humidity condition, the 930.75  $\text{cm}^{-1}$  line is not isolated from H<sub>2</sub>O,  
180 and it improved the retrieval to add the more isolated one at 929.9  $\text{cm}^{-1}$  (see Figure 2). The main interfering species  
181 in MW1 are CO<sub>2</sub>, N<sub>2</sub>O, and H<sub>2</sub>O. Minor interfering species are SF<sub>6</sub> and CFC-12. The second window is spanning  
182 the NH<sub>3</sub> line at 967.35  $\text{cm}^{-1}$ . Again, different widths are used for Bremen/Lauder [966.97-967.68, MW2] and  
183 Reunion Island/Jungfrauoch [962.7-970, MW2]. The very weak absorption signatures at Reunion Island and  
184 Jungfrauoch are close to the noise level and therefore the whole NH<sub>3</sub> absorption shape is retrieved (about 964-  
185 968  $\text{cm}^{-1}$ , see Figure 2) rather than a single line. The main interfering species in MW2 are O<sub>3</sub>, CO<sub>2</sub> and H<sub>2</sub>O for  
186 all sites. At Reunion Island HDO is also interfering in MW2 as well as the isotopologue <sup>686</sup>O<sub>3</sub> (i.e. <sup>16</sup>O-<sup>18</sup>O-<sup>16</sup>O),  
187 which has been fitted in addition to the main <sup>666</sup>O<sub>3</sub>. At Jungfrauoch apart from CO<sub>2</sub>, two O<sub>3</sub> isotopologues (the  
188 most abundant and <sup>686</sup>O<sub>3</sub>) and water vapour which are the main interferences, N<sub>2</sub>O, CFC-12, SF<sub>6</sub> and HDO  
189 absorptions are also retrieved. Typical NH<sub>3</sub> absorptions are weak, on the order of a few tenths of a percent. The

190 typical measurement noise (signal-to-noise ratio) differs per spectra and site but ranges between ~250 at Lauder  
191 to ~450 at Bremen. Channelling was not an issue in any of the spectra and did not need to be fitted.

192

193 Except at Jungfraujoch where SFIT2 is used, the retrieval is performed using the more recent SFIT4.0.9.4  
194 algorithm (Pougatchev et al., 1995, Hase et al., 2004, 2006). Both versions use a form of the optimal estimation  
195 method (Rodgers et al., 2000) to retrieve the volume mixing ratios and total columns of NH<sub>3</sub> and makes use of  
196 a-priori information (profile and covariance matrix). For Bremen, Lauder and Jungfraujoch the used NH<sub>3</sub> a-  
197 priori volume mixing ratios are based on balloon observations (Toon et al. 1999, NH<sub>3</sub> available in dataset but  
198 not reported). The shape of the balloon measurements profile was kept constant but extended and scaled to  
199 expected surface concentrations. The a-priori surface volume mixing ratio is estimated to be 10 ppb for Bremen  
200 (Dämmgen et al., 2005). Although the shape of NH<sub>3</sub> profiles do change through time, the largest share of NH<sub>3</sub> is  
201 expected to be in the mixing layer, which is represented by the lowest layers in the calculation (Van Damme et  
202 al 2014c, Nowak et al., 2010). At Reunion Island, the a priori profile was taken from the MOZART model  
203 (Louisa Emmons, private communication). The a-priori profile peaks at a higher altitude (4-5 km) instead of the  
204 boundary layer as in Bremen, as NH<sub>3</sub> is expected to originate mainly from transport of biomass burning  
205 emissions at this location. At all stations, the a-priori profiles of the interfering species were taken from the  
206 Whole Atmosphere Community Climate Model (Chang et al., 2008).

207

208 At Bremen and Lauder, the a priori covariance matrices only have diagonal values corresponding to standard  
209 deviations of 100% for all layers with no interlayer correlation, chosen in relation to the large range of possible  
210 concentrations and variations between layers. At Jungfraujoch and Reunion Island, we did not use the a priori  
211 covariance matrix as in optimal estimation but the Tikhonov type L<sub>1</sub> regularization (e.g. Sussmann et al., 2009)  
212 was adopted for the Jungfraujoch retrievals. After several tests, values of 50 and 250 were adopted for the alpha  
213 parameter and the signal to noise for inversion, respectively. A Tikhonov regularization with an alpha parameter  
214 value of 50 was also adopted for the Reunion retrievals. The signal to noise ratio is calculated for each spectra,  
215 the mean value being 365.

216

217 Daily temperature and pressure profiles for the meteorological variables were taken from NCEP (National  
218 Center for Environment Prediction). For the radiative transfer calculations the profiles were split into about 50  
219 levels, depending slightly on the station, from ground up to 80 kilometres (100 kilometres in the case of  
220 Jungfraujoch and Reunion Island). The layers have a typical thickness of 500 meters in the troposphere up to 2  
221 km for the higher layers. For the line spectroscopy we use the HITRAN 2012 database (Rothman et al., 2013) in  
222 combination with a number of corrections for CO<sub>2</sub> (ATMOS, Brown et al., 1996) (except for Jungfraujoch for  
223 which the HITRAN lines are used) and sets of pseudo lines generated by G.C. Toon (NASA-JPL) to account for  
224 broad unresolved absorptions by heavy molecules (e.g. CFC-12, SF6).

225

226 Figure 3 shows an example of the fit in both micro windows for the same measured spectra as used in Figure 1.  
227 The top two and bottom two panels show the calculated (Green line) and measured spectrum (Blue line) and the  
228 residual of both micro windows. The simultaneous fits are good with a standard deviation of 0.15% in both  
229 cases.



### 231 **3. Results of the FTIR retrievals**

#### 232 **3.1 Characteristics of the NH<sub>3</sub> retrievals**

##### 233 **3.1.1 Vertical Information**

234 The retrieved vertical information differs from station to station. The top of Figure 4 shows for the 4 stations the  
235 average NH<sub>3</sub> volume mixing ratios (VMR) for each of the retrieved layers (blue line) and the a priori profile that  
236 was used as input in the retrieval (green line). The bottom of Figure 4 shows the averaging kernels for each of the  
237 4 stations averaged over all available observations. As mentioned earlier most of the NH<sub>3</sub> at Bremen is in the  
238 lowest layers. In Figure 4 this is also observed as the averaging kernel shows the most sensitivity in the lowest  
239 layers (red and green lines for the layers 0.03-0.5km and 0.5-1km). The combination of the two spectral micro  
240 windows on average contain 1.9 degree of freedom for signal (DOFS) for the Bremen spectra, which means around  
241 two independent vertical layers can be retrieved. The two separate layers consist of a layer covering ground-1km  
242 and one that covers 1 km - 6 km height, which can be observed in Figure 4. It must be taken into account however  
243 that the shown averaging kernels are a mean for all observations and thus the retrievable number of layers and  
244 combined layer depths vary from spectra to spectra. On average, the Lauder spectra have a DOFS of 1.4. There is  
245 only vertical information for multiple layers during periods with increased NH<sub>3</sub> total columns, which mostly occur  
246 during summer. Similar to Bremen averaging kernels peak near the surface. At Reunion Island only 1.0 DOFS is  
247 achieved, with almost no vertical information available. All the averaging kernels are peaking at the same altitude  
248 (about 5km), which is also the peak of the a priori profile (Figure 4). Similar to the Reunion spectra the  
249 Jungfraujoch spectra do not have vertical information with a DOF of 1.0.

250

##### 251 **3.1.2 Uncertainties Budget**

252 For the error analysis the posteriori error calculation included in the SFIT4 package is used. The error calculation  
253 is based on the error estimation approach by Rodgers (2000). It allows the calculation of the error by attributing  
254 errors to each of the parameters used in the retrieval. The error budget can be divided into three contributions, the  
255 error due to the forward model parameters, the measurement noise and the error due to the vertical resolution of  
256 the retrieval (smoothing error). The assumed uncertainties for the used parameters in the retrieval are listed in  
257 Table 3 for the parameters used in the calculation for Bremen, Lauder and Reunion. For Jungfraujoch, the error  
258 computation was performed using the perturbation method, the spectra of 2009 to 2011 and the Rodger formalism  
259 as explained e.g. in Franco et al., 2015. For Reunion Island, the covariance matrix used for the smoothing error  
260 has diagonal elements representing 150% of variability from the a priori profile. To reflect the error in the NCEP  
261 temperature profiles we assume an uncertainty of about 2 K in the troposphere and a 5 K uncertainty in the  
262 stratosphere. For the uncertainty in the NH<sub>3</sub> line parameters we assume values as stated in the HITRAN 2012  
263 database. We assume a conservative 20% uncertainty for the intensity and 10% for both the temperature and  
264 pressure broadening coefficients.

265

266 The results of the error calculation are listed in in Table 4. Combining the systematic and random errors we have  
267 a mean total error of 25.8 % for all the spectra measured at Bremen (N=554), 30.2 % for the spectra from Lauder  
268 (N=2412), 25.2 % for the Reunion spectra (N=1262) and 34.2 for the Jungfraujoch spectra (N=2702). The errors  
269 are dominated by uncertainties in the spectroscopy. In detail, the random error sources amount to a mean error of  
270 9.1 % for the Bremen spectra, which is mostly due to uncertainty in temperature, measurement noise and the zero



271 level of the sensor (i.e. an instrument property). In the case of the systematic error, with a mean error of 23.5 %,  
272 the error is for the largest part due to the spectroscopy (i.e. line parameters) with smaller contributions of the  
273 temperature, zero level, phase and the smoothing error. The results are similar for the Lauder, Reunion and  
274 Jungfraujoch spectra with most of the uncertainty coming from the line parameters. Hence, line intensity  
275 parameters of the ammonia absorption lines are critical for the  $\text{NH}_3$  concentrations.

276

### 277 **3.2 Time series**

278 Figure 5 shows the  $\text{NH}_3$  total columns retrieved from all available spectra from 2004-2013. Table 5 gives a  
279 summary of statistics of the retrieved  $\text{NH}_3$  columns. Individual measurements at Bremen (blue) show high  
280 concentrations, especially in spring with an overall mean column total of  $13.7\text{e}15$  molecules  $\text{NH}_3 \text{ cm}^{-2}$  and a root  
281 mean square (RMS) of 20.22 indicating a large variability in the observations. The amplitude of the spring peaks  
282 vary throughout the years, with maxima in 2010 and 2013 reaching  $\sim 93\text{e}15$  and  $85\text{e}15$  molecules  $\text{NH}_3 \text{ cm}^{-2}$ . The  
283 variability through the years is caused by changes in meteorology, emissions and timing of the measurements.  
284 Gaps in the data are due to days with overcast and instrument downtimes. The individual observed columns are  
285 sorted into monthly averages to analyse the seasonal variability and to understand the processes driving the  $\text{NH}_3$   
286 concentrations. This is shown in Figure 6 together with monthly averages of surface temperature and CO total  
287 columns.  $\text{NH}_3$  column total concentrations at Bremen (Blue line) have a seasonal cycle with highest levels during  
288 spring, the summer months and autumn. The maximum concentrations occur around April which is consistent  
289 with temporal emission patterns for manure application reported for this region (Friedrich and Reis, 2004; Martin  
290 et al., 2015; Paulot et al., 2014). The baseline variability with higher concentrations in summer can be explained  
291 by an increase in volatilization rates of  $\text{NH}_3$ , emitted from livestock housing, which is driven by animal activity  
292 and temperature (Gyldenkaerne et al., 2005). A comparison with CO is made to distinguish between agricultural  
293 and fire emissions sources. A correlation between  $\text{NH}_3$  and CO columns is not observed, which is consistent with  
294 agriculture as the dominant source of ammonia.

295

296 On average the measurements at Lauder (Figure 5, red line, top panel) yield a column total of  $4.17\text{e}15$  molecules  
297  $\text{NH}_3 \text{ cm}^{-2}$ . These levels are about  $1/3^{\text{rd}}$  of the concentrations measured at Bremen (blue, top panel). Spectra from  
298 Lauder are available for most days in the retrieved time series, which makes it easier to discern peaks and  
299 variability. Distinctive peaks are only visible in the summers. Maxima during spring times are not often observed.  
300 The peak values are similar in between years, with maxima typically around  $30\text{e}15$  molecules  $\text{NH}_3 \text{ cm}^{-2}$ . The RMS  
301 of 5.95 reflects a large variability in the observations between individual retrievals. The average error is  $1.34\text{e}15$   
302 molecules  $\text{NH}_3 \text{ cm}^{-2}$ , which is around a quarter of the mean. Figure 6 shows the seasonal cycle of Lauder (red  
303 line, top left panel). The seasonal variation of  $\text{NH}_3$  coincides with that of the atmospheric temperature (red line,  
304 bottom right panel) and with the livestock emissions in the surrounding region, which are strongly correlated with  
305 temperature.

306

307 The third panel of Figure 5 shows the observations from Reunion (green symbols, bottom panel). The mean  
308 column total observed at Reunion is  $0.80\text{e}15$  molecules  $\text{NH}_3 \text{ cm}^{-2}$ . The concentrations are low during most of the  
309 year. However, peaks reaching densities of  $\sim 6\text{e}15$  molecules  $\text{NH}_3 \text{ cm}^{-2}$  can be observed during the end of each  
310 year. The peaks in September-November coincide with the dry season indicating that emissions are mostly due to

311 biomass burning and large fire events (Vigouroux et al., 2012). This is supported by the increased CO  
312 concentrations, which are also observed in October and November (see, bottom left panel, Figure 6). NH<sub>3</sub> surface  
313 concentration measurements are not available for this region but a recent paper by Van Damme et al. (2015),  
314 which uses IASI-NH<sub>3</sub> observations, shows similar seasonal cycles for the south eastern parts of Africa  
315 (Madagascar). Temperature is almost constant throughout the year and not a major factor in the seasonality of  
316 Reunion.

317  
318 Observations from Jungfraujoch have the lowest mean concentration of all four stations (Figure 5, orange line),  
319 with a mean of 0.18e15 molecules NH<sub>3</sub> cm<sup>-2</sup>. The low concentrations at Jungfraujoch are expected, as the station  
320 is located in the free troposphere high above the surrounding valleys. Transport of NH<sub>3</sub> from the valleys only  
321 occurs sporadically during days with intense vertical mixing. This was also observed in an earlier study of CO  
322 concentrations (Barret et al., 2003). The Jungfraujoch observations show almost no seasonal effects with only a  
323 minimal increase during the summer months. The low concentrations measured at Jungfraujoch support our  
324 assumption on the vertical distribution of the ammonia concentrations with low values in the troposphere that  
325 were used in our a-priori.

326

#### 327 4. Conclusions and perspectives

328

329 In this study we presented a new method to retrieve ammonia total columns from ground-based FTIR solar spectra.  
330 Observations from four complementary stations were used to illustrate the capabilities of the retrieval method.  
331 NH<sub>3</sub> total columns ranging three orders of magnitude were obtained with high abundances at Bremen (mean of  
332 13.7e15 molecules cm<sup>-2</sup>, with a mean DOFS 1.9) to low columns at Jungfraujoch (mean of 0.18e15 molecules cm<sup>-2</sup>,  
333 with a mean DOFS 1.0). The very low levels obtained at the Jungfraujoch demonstrate the sensitivity of the  
334 retrieval method we developed. A separate error calculation shows random errors in the order of 10% and  
335 systematic errors of 25% for individual observations. The errors are dominated by uncertainties in spectroscopy,  
336 atmospheric temperature and deviations in instrumental parameters. For conditions with high surface  
337 concentrations of ammonia, as in Bremen, it is possible to retrieve information on the vertical gradient as two  
338 layers can be discriminated. At Bremen, the retrieval there is most sensitive to ammonia in the planetary boundary  
339 layer, where most of the ammonia is expected. For conditions with lower concentrations there is not enough  
340 information to discriminate individual layers. Station specific seasonal cycles were found to be consistent with  
341 known seasonal cycles of the dominant ammonia sources in the station surroundings. For example, highest levels  
342 in Bremen were observed during spring time when manure is applied to the fields with column total concentrations  
343 reaching up to 93e15 molecules cm<sup>-2</sup>.

344 Remote sensing techniques avoid sampling artefacts common to other techniques such as filter packs (Puchalski  
345 et al., 2011; Bobruzki et al., 2010). For in-situ observations open path remote sensing techniques, e.g. DOAS and  
346 QCL instruments, are starting to be used (Volten et al., 2010, Miller et al., 2014). The FTIR-NH<sub>3</sub> observations  
347 would be an excellent addition to these approaches as it provides the NH<sub>3</sub> total column and profiles, including  
348 vertical information for sites sampling high ammonia levels. With a mean error of ~25% for all observations in  
349 high ammonia source areas the accuracy of the FTIR retrievals is comparable to that reported for satellite products  
350 (TES, IASI, CrIS). Compared to the in-situ open path remote sensing methods the FTIR method has a higher

351 uncertainty, but this is a trade-off for the ability to retrieve vertical information. To improve the accuracy of the  
352 FTIR-NH<sub>3</sub> retrieval a reassessment of the spectral line parameters is necessary.

353 Observations from existing networks commonly represent daily or even monthly averaged concentration values,  
354 which severely complicates any attempt to validate satellite observations. The novel FTIR-NH<sub>3</sub> observations  
355 enable a direct validation of satellite products. As the FTIR- NH<sub>3</sub> product provides averaging kernels a direct  
356 comparison can be made with optimal estimation satellite retrievals while taking account of the a-priori  
357 information and vertical sensitivity of both instruments (Rogers and Connor, 2003). A dedicated field campaign  
358 was executed at the Cabauw Experimental Site for Atmospheric Remote Sensing (CESAR) in the Netherlands  
359 (spring and summer 2014) to validate the IASI- NH<sub>3</sub> using a range of instruments including mini-DOAS  
360 instruments and a Bruker IFS-66 instrument (Dammers et al. in prep).

361 The uncertainty in the emission distributions hampers the performance and prediction capabilities of air quality  
362 and climate models (Heald et al., 2012). Emissions are usually based on nationally reported yearly emission  
363 inventories (Pouliot et al., 2012) and gridded by distributing the emissions following animal numbers and  
364 agricultural land use (Bouwman et al., 2002, Keunen et al., 2011). To improve on static emission time profiles, a  
365 new direction is to include the impact of meteorological variability of ammonia emissions in modelling systems  
366 (Sutton et al., 2013). Recently, such an improvement was shown to greatly enhance the performance of air quality  
367 models (Skjoth et al., 2011). Satellite observations in combination with chemical transport models (CTM) have  
368 been used to provide a top-down constraint on ammonia emissions (e.g. Zhu et al., 2013). Similar to satellite  
369 observations, FTIR total columns in combination with surface and satellite observations could provide the means  
370 to evaluate the emission modelling through comparing trends and concentration anomalies within and between  
371 years. For this purpose continuous time series are necessary. Due to the lack of continuous data (i.e. more than  
372 one observation per hour) we could not derive a typical diurnal cycle in this study, whereas this would be highly  
373 useful for model evaluation. Improved knowledge on the diurnal cycles may also greatly help to interpret model  
374 evaluation results against satellite data as they provide snapshots, e.g. daily IASI's observations at 9:30 local time.  
375 Also, the model-measurement comparison would be less sensitive to modelling errors in the turbulent vertical  
376 exchange as the ammonia is integrated over vertical.

377 The developed retrieval methodology from FTIR-instruments provides a new way to obtain vertically and  
378 temporally resolved measurements on ammonia concentrations. FTIR-NH<sub>3</sub> observations may prove very valuable  
379 for satellite and model validation and may provide a complementary source of information to constrain the global  
380 ammonia budget.

### 381 **Acknowledgements**

382 This work is part of the research programme GO/12-36, which is financed by the Netherlands Organisation for  
383 Scientific Research (NWO). Acknowledgements are addressed to the Université de La Réunion and CNRS  
384 (LACy-UMR8105 and UMS3365) for their strong support of the OPAR station (Observatoire de Physique de  
385 l'Atmosphère de la Réunion) and the OSU-R (Observatoire des Sciences de l'Univers de la Réunion)  
386 activities. The authors gratefully acknowledge C. Hermans and F. Scolas from BIRA-IASB, and J.-M. Metzger  
387 from Université de La Réunion, for the Reunion Island measurements. We are also grateful to Louisa Emmons

388 (NCAR) who provided NH<sub>3</sub> profiles from the MOZART model used as a priori in the Reunion Island retrievals.  
389 The University of Liège contribution to the present work has mainly been supported by the A3C project (PRODEX  
390 Program of the Belgian Science Policy Office, BELSPO, Brussels). Additional support was provided by  
391 MeteoSwiss (Global Atmospheric Watch), the Fédération Wallonie-Bruxelles and the F.R.S. – FNRS. We thank  
392 the International Foundation High Altitude Research Stations Jungfrauoch and Gornergrat (HFSJG, Bern). E.  
393 Mahieu is Research Associate with F.R.S. – FNRS. The Lauder NIWA FTIR program is funded through the New  
394 Zealand Government's core research grant framework. We are grateful to the many colleagues who have  
395 contributed to FTIR data acquisition at the various sites.

396  
397  
398

## References

- 399 Barret, B., De Mazière, M., and Mahieu, E.: Ground-based FTIR measurements of CO from the Jungfrauoch:  
400 characterisation and comparison with in situ surface and MOPITT data, *Atmos. Chem. Phys.*, 3, 2217-2223,  
401 doi:10.5194/acp-3-2217-2003, 2003.
- 402
- 403 Bobbink, R., Hornung, M., & Roelofs, J. G. (1998). The effects of air-borne nitrogen pollutants on species  
404 diversity in natural and semi-natural European vegetation. *Journal of Ecology*, 86(5), 717-738.
- 405
- 406 Bobbink, R, Hicks K, Galloway J, Spranger T, Alkemade R, Ashmore M, Bustamante M, Cinderby S, Davidson  
407 E, Dentener F, Emmett B, Erisman JW, Fenn M, Gilliam F, Nordin A, Pardo L, De Vries W. Global assessment  
408 of nitrogen deposition effects on terrestrial plant diversity: a synthesis, *Ecological Applications*, 20 (2010), pp.  
409 30–59
- 410
- 411 von Bobruzki, K., Braban, C. F., Famulari, D., Jones, S. K., Blackall, T., Smith, T. E. L., Blom, M., Coe, H.,  
412 Gallagher, M., Ghalaieny, M., McGillen, M. R., Percival, C. J., Whitehead, J. D., Ellis, R., Murphy, J.,  
413 Mohacsi, A., Pogany, A., Junninen, H., Rantanen, S., Sutton, M. A., and Nemitz, E.: Field inter-comparison of  
414 eleven atmospheric ammonia measurement techniques, *Atmos. Meas. Tech.*, 3, 91-112, doi:10.5194/amt-3-91-  
415 2010, 2010.
- 416 Bouwman, A. F., Lee, D. S., Asman, W. A. H., Dentener, F. J., Van Der Hoek, K. W., & Olivier, J. G. J. (1997).  
417 A global high-resolution emission inventory for ammonia. *Global biogeochemical cycles*, 11(4), 561-587.
- 418 Bouwman, A. F., L. J. M. Boumans, and N. H. Batjes (2002), Estimation of global NH<sub>3</sub> volatilization loss from  
419 synthetic fertilizers and animal manure applied to arable lands and grasslands, *Global Biogeochem. Cycles*, 16(2),  
420 1024, doi:10.1029/2000GB001389.
- 421 Brown, L. R., M. R. Gunson, R. A. Toth, F. W. Irion, C. P. Rinsland, and A. Goldman. "1995 atmospheric trace  
422 molecule spectroscopy (ATMOS) linelist." *Applied optics* 35, no. 16 (1996): 2828-2848.
- 423 Chang, L., Palo, S., Hagan, M., Richter, J., Garcia, R., Riggin, D. and Fritts, D.: Structure of the migrating diurnal  
424 tide in the Whole Atmosphere Community Climate Model (WACCM), *Advances in Space Research*, 41(9), 1398–  
425 1407, doi:10.1016/j.asr.2007.03.035, 2008.
- 426 Charlson, R. J., Langner, J., Rodhe, H., Leovy, C. B., and Warren, S. G.: Perturbation of the Northern-Hemisphere  
427 radiative balance by backscattering from anthropogenic sulfate 15 aerosols, *Tellus A*, 43, 152–163, 1991.
- 428 Clarisse, Lieven, Cathy Clerbaux, Frank Dentener, Daniel Hurtmans, and Pierre-François Coheur. "Global  
429 ammonia distribution derived from infrared satellite observations." *Nature Geoscience* 2, no. 7 (2009): 479-483.
- 430 Dämmgen, U., & Erisman, J. W. (2005). Emission, transmission, deposition and environmental effects of  
431 ammonia from agricultural sources. *Kuczynski, T.; Dämmgen, U.; Webb, J*, 97-112.
- 432 Dentener, F., Drevet, J., Lamarque, J. F., Bey, I., Eickhout, B., Fiore, A. M., et al. (2006). Nitrogen and sulfur  
433 deposition on regional and global scales: A multimodel evaluation. *Global Biogeochemical Cycles*, 20: GB4003.  
434 doi:10.1029/2005GB002672.

435 Dils, B., De Mazière, M., Müller, J. F., Blumenstock, T., Buchwitz, M., de Beek, R., Demoulin, P., Duchatelet, P.,  
436 Fast, H., Frankenberg, C., Gloudemans, A., Griffith, D., Jones, N., Kerzenmacher, T., Kramer, I., Mahieu, E.,  
437 Mellqvist, J., Mittermeier, R. L., Notholt, J., Rinsland, C. P., Schrijver, H., Smale, D., Strandberg, A.,  
438 Straume, A. G., Stremme, W., Strong, K., Sussmann, R., Taylor, J., van den Broek, M., Velazco, V., Wagner, T.,  
439 Warneke, T., Wiacek, A., and Wood, S.: Comparisons between SCIAMACHY and ground-based FTIR data for  
440 total columns of CO, CH<sub>4</sub>, CO<sub>2</sub> and N<sub>2</sub>O, *Atmos. Chem. Phys.*, 6, 1953-1976, doi:10.5194/acp-6-1953-2006,  
441 2006.

442 EDGAR-Emission Database for Global Atmospheric Research: Source: EC-JRC/PBL. EDGAR version 4.2.,  
443 <http://edgar.jrc.ec.europa.eu>, access 15th October 2012, 2011  
444

445 Erisman, J. W., Vermetten, A. W., Asman, W. A., Waijers-Ijpelaar, A., & Slanina, J. (1988). Vertical distribution  
446 of gases and aerosols: the behaviour of ammonia and related components in the lower atmosphere. *Atmospheric*  
447 *Environment (1967)*, 22(6), 1153-1160.

448 Erisman, J. W., Otjes, R., Hensen, A., Jongejan, P., van den Bulk, P., Khlystov, A., Mols, H., and Slanina, J.:  
449 Instrument development and application in studies and monitoring of ambient ammonia, *Atmos. Environ.*, 35,  
450 1913–1922, 2001.

451 Erisman, J. W., Bleeker, A., Galloway, J., & Sutton, M. S. (2007). Reduced nitrogen in ecology and the  
452 environment. *Environmental Pollution*, 150(1), 140-149.

453 Fowler, D., Coyle, M., Skiba, U., Sutton, M. A., Cape, J. N., Reis, S., Sheppard, L. J., Jenkins, A., Grizzetti, B.,  
454 Galloway, J. ., Vitousek, P., Leach, A., Bouwman, A. F., Butterbach-Bahl, K., Dentener, F., Stevenson, D.,  
455 Amann, M., and Voss, M.: The global nitrogen cycle in the twenty-first century, *Philos. Trans. R. Soc. London*,  
456 *Ser. B*, 368, Doi:10.1098/rstb.2013.0164, 2013.  
457

458 Franco, B., Hendrick, F., Van Roozendaal, M., Müller, J.-F., Stavrou, T., Marais, E. A., Bovy, B., Bader, W.,  
459 Fayt, C., Hermans, C., Lejeune, B., Pinardi, G., Servais, C. and Mahieu, E.: Retrievals of formaldehyde from  
460 ground-based FTIR and MAX-DOAS observations at the Jungfraujoch station and comparisons with GEOS-  
461 Chem and IMAGES model simulations, *Atmospheric Measurement Techniques*, 8(4), 1733–1756,  
462 doi:10.5194/amt-8-1733-2015, 2015.  
463

464 Friedrich, R., & Reis, S. (Eds.). (2004). *Emissions of air pollutants*. Springer Science & Business Media.  
465

466 Gyldenkerne, S., Ambelas Skjøth, C., Hertel, O., & Ellermann, T. (2005). A dynamical ammonia emission  
467 parameterization for use in air pollution models. *Journal of Geophysical Research: Atmospheres (1984–*  
468 *2012)*, 110(D7).  
469

470 Griffith, D. W. T., Jones, N. B., McNamara, B., Walsh, C. P., Bell, W., and Bernardo, C.: Intercomparison of  
471 NDSC ground-based solar FTIR measurements of atmospheric gases at Lauder, New Zealand, *J. Atmos. Ocean.*  
472 *Tech.*, 20, 1138–1153, 2003.  
473

474 Griesfeller, a., Griesfeller, J., Hase, F., Kramer, I., Loès, P., Mikuteit, S., Raffalski, U., Blumenstock, T. and  
475 Nakajima, H.: Comparison of ILAS-II and ground-based FTIR measurements of O<sub>3</sub>, HNO<sub>3</sub>, N<sub>2</sub>O, and CH<sub>4</sub>  
476 over Kiruna, Sweden, *J. Geophys. Res.*, 111(D11), D11S07, doi:10.1029/2005JD006451, 2006.  
477

478 Hansen, D. A., E. S. Edgerton, B. E. Hartsell, J. J. Jansen, N. Kandasamy, G. M. Hidy, and C. L. Blanchard (2003),  
479 The southeastern aerosol research and characterization study: Part 1. Overview, *J. Air Waste Manage. Assoc.*, 53,  
480 1460–1471, doi:10.1080/10473289.2003.10466318.  
481

482 Hase, F.; Blumenstock, T. & Paton-Walsh, C. Analysis of the instrumental line shape of high-resolution Fourier  
483 transform IR spectrometers with gas cell measurements and new retrieval software *Appl. Opt.*, 1999, 38

484 Hase, F., et al. "Intercomparison of retrieval codes used for the analysis of high-resolution, ground-based FTIR  
485 measurements." *Journal of Quantitative Spectroscopy and Radiative Transfer* 87.1 (2004): 25-52.  
486

487 Hase, F., Demoulin, P., Sauval, A. J., Toon, G. C., Bernath, P. F., Goldman, A., Hannigan, J. W., Rinsland, C. P.:  
488 An empirical line-by-line model for the infrared solar transmittance spectrum from 700 to 5000 cm<sup>-1</sup>, *J. Quant.*  
489 *Spectrosc. Ra.*, 102, 450–463, doi:10.1016/j.jqsrt.2006.02.026, 2006.

491 Heald, C. L., Jr., J. L. C., Lee, T., Benedict, K. B., Schwandner, F. M., Li, Y., Clarisse, L., Hurtmans, D. R.,  
492 Van Damme, M., Clerbaux, C., Coheur, P.-F., Philip, S., Martin, R. V., and Pye, H. O. T.: Atmospheric  
493 ammonia and particulate inorganic nitrogen over the United States, *Atmos. Chem. Phys.*, 12, 10 295–10 312,  
494 doi:10.5194/acp-12-10295-2012, 2012.

495  
496 Holland, E. A., Dentener, F. J., Braswell, B. H., & Sulzmann, J. M. (1999). Contemporary and pre-industrial global  
497 reactive nitrogen budgets. In *New Perspectives on Nitrogen Cycling in the Temperate and Tropical Americas* (pp.  
498 7-43). Springer Netherlands.

499  
500 Kerzenmacher, T., Dils, B., Kumps, N., Blumenstock, T., Clerbaux, C., Coheur, P.-F., Demoulin, P., García, O.,  
501 George, M., Griffith, D. W. T., Hase, F., Hadji-Lazaro, J., Hurtmans, D., Jones, N., Mahieu, E., Notholt, J., Paton-  
502 Walsh, C., Raffalski, U., Ridder, T., Schneider, M., Servais, C., and De Mazière, M.: Validation of IASI FORLI  
503 carbon monoxide retrievals using FTIR data from NDACC, *Atmos. Meas. Tech.*, 5, 2751-2761, doi:10.5194/amt-  
504 5-2751-2012, 2012.

505  
506 Kuenen, J., H. Denier van der Gon, A. Visschedijk, H. van der Brugh, and R. van Gijlswijk (2011), MACC  
507 European emission inventory for the years 2003–2007, *TNO Rep. TNO-060-UT-2011-00588*, TNO, Utrecht,  
508 Netherlands.

509  
510 Mount, G. H., Rumburg, B., Havig, J., Lamb, B., Westberg, H., Yonge, D., Johnson, K., and Kincaid, R.:  
511 Measurement of atmospheric ammonia at a dairy using differential optical absorption spectroscopy in the mid-  
512 ultraviolet, *Atmos. Environ.*, 36, 1799–1810, 2002.

513  
514 Krupa, S.: Effects of atmospheric ammonia (NH<sub>3</sub>) on terrestrial vegetation: a review, *Environ. Pollut.*, 124, 179  
515 – 221, doi:http://dx.doi.org/10.1016/S0269-7491(02)00434-7, 2003.

516  
517 Leen, J. B., Yu, X. Y., Gupta, M., Baer, D. S., Hubbe, J. M., Kluzek, C. D., ... & Hubbell, M. R. (2013). Fast In  
518 Situ Airborne Measurement of Ammonia Using a Mid-Infrared Off-Axis ICOS Spectrometer. *Environmental*  
519 *science & technology*, 47(18), 10446-10453.

520  
521 Luo, M., Shephard, M. W., Cady-Pereira, K. E., Henze, D. K., Zhu, L., Bash, J. O., Pinder, R. W., Capps, S., and  
522 Walker, J.: Satellite Observations of Tropospheric Ammonia and Carbon Monoxide: Global Distributions,  
523 Correlations and Comparisons to Model Simulations, *Atmos. Environ.*, 106, 262–277,  
524 doi:10.1016/j.atmosenv.2015.02.007, 2015

525  
526 Miller, D. J., Sun, K., Tao, L., Khan, M. A., and Zondlo, M. A.: Open-path, quantum cascade-laser-based sensor  
527 for high-resolution atmospheric ammonia measurements, *Atmos. Meas. Tech.*, 7, 81-93, doi:10.5194/amt-7-81-  
528 2014, 2014.

529  
530 Mount G H, Rumburg B, Havig J, Lamb B, Westberg H, Yonge D, Johnson K and Kincaid R 2002 Measurement  
531 of atmospheric ammonia at a dairy using differential optical absorption spectroscopy in the mid-ultraviolet *Atmos.*  
532 *Environ.* **36** 1799–810

533  
534 Nowak, J. B., Neuman, J. A., Kozai, K., Huey, L. G., Tanner, D. J., Holloway, J. S., Ryerson, T. B., Frost, G. J.,  
535 McKeen, S. A., and Fehsenfeld, F. C.: A chemical ionization mass spectrometry technique for airborne  
536 measurements of ammonia, *J. Geophys. Res.-Atmos.*, 112, D10S02, doi:10.1029/2006JD007589, 2007.

537  
538 Nowak, J. B., Neuman, J. A., Bahreini, R., Brock, C. A., Middlebrook, A. M., Wollny, A. G., Holloway, J. S.,  
539 Peischl, J., Ryerson, T. B., and Fehsenfeld, F. C.: Airborne observations of ammonia and ammonium nitrate  
540 formation over Houston, Texas, *J. Geophys. Res.-Atmos.*, 115, D22 304, doi:10.1029/ 2010JD014195, 2010.

541  
542 Rodgers, Clive D. *Inverse methods for atmospheric sounding: theory and practice*. Vol. 2. Singapore: World  
543 scientific, 2000.

544  
545 Rodhe, H., Dentener, F., & Schulz, M. (2002). The global distribution of acidifying wet deposition. *Environmental*  
546 *Science & Technology*, 36(20), 4382-4388.

547  
548 Rothman, L. S., I. E. Gordon, Y. Babikov, A. Barbe, D. Chris Benner, P. F. Bernath, Manfred Birk et al. "The  
549 HITRAN2012 molecular spectroscopic database." *Journal of Quantitative Spectroscopy and Radiative*  
550 *Transfer* 130 (2013): 4-50.

551  
552 Paton-Walsh, C., Jones, N. B., Wilson, S. R., Haverd, V., Meier, A., Griffith, D. W., and Rinsland, C. P. (2005).  
553 Measurements of trace gas emissions from Australian forest fires and correlations with coincident measurements  
554 of aerosol optical depth. *Journal of Geophysical Research: Atmospheres (1984–2012)*, 110(D24).  
555

556 Paulot, F., D. J. Jacob, R. W. Pinder, J. O. Bash, K. Travis, and D. K. Henze (2014), Ammonia emissions in the  
557 United States, European Union, and China derived by high resolution inversion of ammonium wet deposition  
558 data: Interpretation with a new agricultural emissions inventory (MASAGE NH3), *J. Geophys. Res.-Atmos.*,  
559 119(7), 4343–4364, doi:10.1002/2013JD021130.  
560

561 Pope, III, C. A., Ezzati, M., and Dockery, D. W.: Fine-Particulate Air Pollution and Life Expectancy in the United  
562 States, *N. Engl. J. Med.*, 360, 376–386, doi:{10.1056/NEJMs0805646}, 2009.  
563

564 Pougatchev, N. S., Connor, B. J., & Rinsland, C. P. (1995). Infrared measurements of the ozone vertical  
565 distribution above Kitt Peak. *Journal of Geophysical Research: Atmospheres (1984–2012)*, 100(D8), 16689-  
566 16697.  
567

568 Pouliot, G., T. Pierce, H. D. van der Gon, M. Schaap, M. Moran, and U. Nopmongcol (2012), Comparing emission  
569 inventories and model-ready emission datasets between Europe and North America for the AQMEII project,  
570 *Atmos. Environ.*, 53(0), 4–14, doi:10.1016/j.atmosenv.2011.12.041.  
571

572 Puchalski, M. A., M. E. Sather, J. T. Walker, C. M. Lehmann, D. A. Gay, J. Mathew, and W. P. Robarge (2011),  
573 Passive ammonia monitoring in the United States: Comparing three different sampling devices, *J. Environ. Monit.*,  
574 13(11), 3156–3167, doi:10.1039/c1em10553a.  
575

576 Rao, K.N., and A. Weber, Spectroscopy of the Earth's Atmosphere and Interstellar Medium, Academic, San Diego,  
577 Calif., 1992

578 Reay, D. S., Dentener, F., Smith, P., Grace, J., & Feely, R. A. (2008). Global nitrogen deposition and carbon  
579 sinks. *Nature Geoscience*, 1(7), 430-437.

580 Rodhe, Henning, Frank Dentener, and Michael Schulz. "The global distribution of acidifying wet  
581 deposition." *Environmental Science & Technology* 36.20 (2002): 4382-4388.

582 Rothman, L. S., Gordon, I. E., Babikov, Y., Barbe, A., Benner, D. C., & Bernath, P. F. (2013). The HITRAN  
583 database: 2012 edition. *J Quant Spectrosc Radiat Transfer*.  
584

585 Rodgers, C. D., & Connor, B. J. (2003). Intercomparison of remote sounding instruments. *Journal of Geophysical*  
586 *Research: Atmospheres (1984–2012)*, 108(D3).  
587

588 Schaap, M., van Loon, M., ten Brink, H. M., Dentener, F. J., and Bultjes, P. J. H.: Secondary inorganic aerosol  
589 simulations for Europe with special attention to nitrate, *Atmos. Chem. Phys.*, 4, 857-874, doi:10.5194/acp-4-857-  
590 2004, 2004  
591

592 Shephard, M. W., Cady-Pereira, K. E., Luo, M., Henze, D. K., Pinder, R. W., Walker, J. T., Rinsland, C. P.,  
593 Bash, J. O., Zhu, L., Payne, V. H., and Clarisse, L.: TES ammonia retrieval strategy and global observations of  
594 the spatial and seasonal variability of ammonia, *Atmos. Chem. Phys.*, 11, 10743-10763, doi:10.5194/acp-11-  
595 10743-2011, 2011.

596 Shephard, M. W. and Cady-Pereira, K. E.: Cross-track Infrared Sounder (CrIS) satellite observations of  
597 tropospheric ammonia, *Atmos. Meas. Tech.*, 8, 1323-1336, doi:10.5194/amt-8-1323-2015, 2015b.

598 Shephard, M. W., McLinden, C. A., Cady-Pereira, K. E., Luo, M., Moussa, S. G., Leithead, A., Liggio, J., Staebler,  
599 R. M., Akingunola, A., Makar, P., Lehr, P., Zhang, J., Henze, D. K., Millet, D. B., Bash, J. O., Zhu, L., Wells, K.  
600 C., Capps, S. L., Chaliyakunnel, S., Gordon, M., Hayden, K., Brook, J. R., Wolde, M., and Li, S.-M.: Tropospheric  
601 Emission Spectrometer (TES) satellite validations of ammonia, methanol, formic acid, and carbon monoxide over  
602 the Canadian oil sands, *Atmos. Meas. Tech. Discuss.*, 8, 9503-9563, doi:10.5194/amtd-8-9503-2015, 2015a.

603 Skjøth, C. A., Geels, C., Berge, H., Gyldenkerne, S., Fagerli, H., Ellermann, T., Frohn, L. M., Christensen, J.,  
604 Hansen, K. M., Hansen, K., and Hertel, O.: Spatial and temporal variations in ammonia emissions – a freely  
605 accessible model code for Europe, *Atmos. Chem. Phys.*, 11, 5221-5236, doi:10.5194/acp-11-5221-2011, 2011.

606 Sussmann, R., Borsdorff, T., Rettinger, M., Camy-Peyret, C., Demoulin, P., Duchatelet, P., Mahieu, E., and  
607 Servais, C.: Technical Note: Harmonized retrieval of column-integrated atmospheric water vapour from the FTIR  
608 network – first examples for long-term records and station trends, *Atmos. Chem. Phys.*, 9, 8987-8999, 2009.  
609

610 Sutton, M. A., et al. (2013), Towards a climate-dependent paradigm of ammonia emission and deposition, *Philos.*  
611 *Trans. R. Soc. London, Ser. B*, 368(1621), 20130166, doi:10.1098/rstb.2013.0166.  
612

613 Thijsse, T. R., Duyzer, J. H., Verhagen, H. L. M., Wyers, G. P., Wayers, A., and Möls, J. J.: Measurement of  
614 ambient ammonia with diffusion tube samplers, *Atmos. Environ.*, 32, 333–337, 1998.  
615

616 Thomas, R. M., Trebs, I., Otjes, R., Jongejan, P. A. C., ten Brink, H., Phillips, G., Kortner, M., Meixner, F. X.,  
617 and Nemitz, E.: An automated analyzer to measure surface-atmosphere exchange fluxes of water soluble inorganic  
618 aerosol compounds and reactive trace gases, *Environ. Sci. Technol.*, 43, 1412–1418, 2009.  
619

620 Toon, G. C., Blavier, J.-F., Sen, B., Margitan, J. J., Webster, C. R., Max, R. D., Fahey, D. W., Gao, R., DelNegro,  
621 L., Proffitt, M., Elkins, J., Romashkin, P. A., Hurst, D. F., Oltmans, S., Atlas, E., Schauffler, S., Flocke, F., Bui,  
622 T. P., Stimpfle, R. M., Bonne, G. P., Voss, P. B., and Cohen, R. C.: Comparison of MkIV balloon and ER-2  
623 aircraft measurements of atmospheric trace gases, *J. Geophys. Res.*, 104, 26 779–26 790, 1999.  
624

625 Van Damme, M., Clarisse, L., Heald, C. L., Hurtmans, D., Ngadi, Y., Clerbaux, C., Dolman, A. J., Erisman, J. W.,  
626 and Coheur, P. F.: Global distributions, time series and error characterization of atmospheric ammonia (NH<sub>3</sub>) from  
627 IASI satellite observations, *Atmos. Chem. Phys.*, 14, 2905-2922, doi:10.5194/acp-14-2905-2014, 2014a.

628 Van Damme, M., R. J. Wichink Kruit, M. Schaap, L. Clarisse, C. Clerbaux, P.-F. Coheur, E. Dammers, A. J.  
629 Dolman, and J. W. Erisman, Evaluating 4 years of atmospheric ammonia (NH<sub>3</sub>) over Europe using IASI satellite  
630 observations and LOTOS-EUROS model results, *J. Geophys. Res. Atmos.*, 119, 9549–9566,  
631 doi:10.1002/2014JD021911, 2014b

632 Van Damme, M., Clarisse, L., Dammers, E., Liu, X., Nowak, J. B., Clerbaux, C., Flechard, C. R., Galy-Lacaux, C.,  
633 Xu, W., Neuman, J. A., Tang, Y. S., Sutton, M. A., Erisman, J. W., and Coheur, P. F.: Towards validation of  
634 ammonia (NH<sub>3</sub>) measurements from the IASI satellite, *Atmos. Meas. Tech. Discuss.*, 7, 12125-12172,  
635 doi:10.5194/amtd-7-12125-2014, 2014c

636 Van Damme, M., Erisman, J. W., Clarisse, L., Dammers, E., Whitburn, S., Clerbaux, C., Dolman, A. J., and  
637 Coheur, P. F., Worldwide spatiotemporal atmospheric ammonia (NH<sub>3</sub>) variability revealed by satellite, *Geophys.*  
638 *Research. Let.* (in revision), 2015.  
639

640 Van Putten, E. M., Mennen, M. G., Regts, T., and Uiterwijk, J. W.: Performance study of four automatic ammonia  
641 monitors under controlled conditions, report 723101004, RIVM, 1994  
642

643 Vigouroux, C., Stavrakou, T., Whaley, C., Dils, B., Duflot, V., Hermans, C., Kumps, N., Metzger, J.-M.,  
644 Scolas, F., Vanhaelewyn, G., Müller, J.-F., Jones, D. B. A., Li, Q., and De Mazière, M.: FTIR time-series of  
645 biomass burning products (HCN, C<sub>2</sub>H<sub>6</sub>, C<sub>2</sub>H<sub>2</sub>, CH<sub>3</sub>OH, and HCOOH) at Reunion Island (21° S, 55° E) and  
646 comparisons with model data, *Atmos. Chem. Phys.*, 12, 10367-10385, doi:10.5194/acp-12-10367-2012, 2012.

647 Vigouroux, 2013, EGU, Ground-based FTIR measurements of NH<sub>3</sub> total columns and comparison with IASI data

648 Vitousek, P.M., Aber, J., Howarth, R. W., Likens, G. E., Matson, P. A., Schindler, D. W., Schlesinger, W. H., &  
649 Tilman, G. D. (1997). *Human alteration of the global nitrogen cycle: causes and consequences*. Washington, DC,  
650 US: Ecological Society of America.

651 Volten, H., Bergwerff, J. B., Haaima, M., Lolkema, D. E., Berkhout, A. J. C., van der Hoff, G. R., Potma, C. J. M.,  
652 Wichink Kruit, R. J., van Pul, W. A. J., and Swart, D. P. J.: Two instruments based on differential optical  
653 absorption spectroscopy (DOAS) to measure accurate ammonia concentrations in the atmosphere, *Atmos. Meas.*  
654 *Tech.*, 5, 413-427, doi:10.5194/amt-5-413-2012, 2012.

655 Whitburn, S., Van Damme, M., Kaiser, J. W., van der Werf, G. R., Turquety, S., Hurtmans, D., Clarisse, L.,  
656 Clerbaux, C., Coheur, P. F. (2015). Ammonia emissions in tropical biomass burning regions: Comparison between  
657 satellitederived emissions and bottom-up fire inventories, *Atmospheric Environment* (2015),  
658 <http://dx.doi.org/10.1016/j.atmosenv.2015.03.015>



- 659 Wood, S. W.: Validation of version 5.20 ILAS HNO<sub>3</sub>, CH<sub>4</sub>, N<sub>2</sub>O, O<sub>3</sub>, and NO<sub>2</sub> using ground-based  
660 measurements at Arrival Heights and Kiruna, *J. Geophys. Res.*, 107(D24), 8208, doi:10.1029/2001JD000581,  
661 2002.  
662
- 663 Yokelson, R. J., Susott, R., Ward, D. E., Reardon, J. and Griffith, D. W. T.: Emissions from smoldering  
664 combustion of biomass measured by open-path Fourier transform infrared spectroscopy, *J. Geophys. Res.*,  
665 102(D15), 18865, doi:10.1029/97JD00852, 1997.
- 666 Yokelson, R., Urbanski, S., Atlas, E., Toohey, D., Alvarado, E., Crouse, J., Wennberg, P., Fisher, M., Wold, C.,  
667 Campos, T., Adachi, K., Buseck, P. R. and Hao, W. M.: Emissions from forest fires near Mexico City, *Atmos.*  
668 *Chem. Phys. Discuss.*, 7(3), 6687–6718, doi:10.5194/acpd-7-6687-2007, 2007.
- 669 Zander, R., Mahieu, E., Demoulin, P., Duchatelet, P., Roland, G., Servais, C., De Mazière, M., Reimann, S.,  
670 and Rinsland, C.P.: Our changing atmosphere: Evidence based on long-term infrared solar observations at the  
671 Jungfraujoch since 1950, *Sci. Total Environ.*, 391, 184-195, 2008.  
672
- 673 Zhu, L., Henze, D. K., Cady-Pereira, K. E., Shephard, M. W., Luo, M., Pinder, R. W., Bash, J. O. and Jeong, G.  
674 R.: Constraining U.S. ammonia emissions using TES remote sensing observations and the GEOS-Chem adjoint  
675 model, *J. Geophys. Res. Atmos.*, 118(8), 3355–3368, doi:10.1002/jgrd.50166, 2013.  
676

**Table 1** FTIR stations used in the analysis. The location, longitude, latitude and altitude are given for each station as well as the instrument used for the measurements. Some station specifics are given in the last column.

Station	Location	Longitude	Latitude	Altitude (m.a.s.l.)	Instrument	Station specifics
Bremen	Germany	8.85E	53.10N	27	Bruker 125 HR	City, fertilizers, livestock
Lauder	New Zealand	169.68E	45.04S	370	Bruker 120 HR	Fertilizers, livestock
Reunion	Indian Ocean	55.5E	20.90S	85	Bruker 120 M	Fertilizers, fires
Jungfrauoch	Switzerland	7.98E	46.55N	3580	Bruker 120 HR	High altitude, no large sources

678

**Table 2** Micro windows used in the NH<sub>3</sub> retrieval at the four stations.

Stations	Micro window	Spectral range (cm <sup>-1</sup> )	Interfering species (Profile retrieved species in <b>bold</b> )	Signal-to-noise ratio (SNR)
Bremen and Lauder	MW1	930.32-931.32	<b>NH<sub>3</sub></b> , <b>H<sub>2</sub>O</b> , <b>O<sub>3</sub></b> , CO <sub>2</sub> , N <sub>2</sub> O, HNO <sub>3</sub> , SF <sub>6</sub> , CFC-12, solar lines	Bremen – Real SNR mean value of 450
	MW2	966.97-967.68	<b>NH<sub>3</sub></b> , <b>H<sub>2</sub>O</b> , <b>O<sub>3</sub></b> , CO <sub>2</sub> , N <sub>2</sub> O, HNO <sub>3</sub> , solar lines	Lauder – Real SNR mean value of 250
Reunion	MW1	929.4-931.4	<b>NH<sub>3</sub></b> , <b>H<sub>2</sub>O</b> , O <sub>3</sub> , CO <sub>2</sub> , N <sub>2</sub> O, HNO <sub>3</sub> , SF <sub>6</sub> , CFC-12	Reunion – Real SNR mean value of 365
	MW2	962.1-970.0	<b>NH<sub>3</sub></b> , <b>H<sub>2</sub>O</b> , O <sub>3</sub> , CO <sub>2</sub> , N <sub>2</sub> O, HNO <sub>3</sub> , HDO, <sup>686</sup> O <sub>3</sub> , solar lines	
Jungfrauoch	MW1	929.4-931.4	<b>NH<sub>3</sub></b> , H <sub>2</sub> O, O <sub>3</sub> , CO <sub>2</sub> , N <sub>2</sub> O, HNO <sub>3</sub> , SF <sub>6</sub> , CFC-12	
	MW2	962.1-970.0	<b>NH<sub>3</sub></b> , H <sub>2</sub> O, O <sub>3</sub> , CO <sub>2</sub> , N <sub>2</sub> O, HDO, <sup>686</sup> O <sub>3</sub> , solar lines	<b>Jungfrauoch – Fixed at 250</b>

679

**Table 3** Random and Systematic uncertainties used in the error calculation

Version (Stations)	SFIT 4 (Bremen, Lauder, Reunion)		Version (Stations)	SFIT 2 (Jungfrauoch)	
Parameter	Random uncertainty	Systematic uncertainty	Parameter	Random uncertainty	Systematic uncertainty
Temperature	2 K troposphere 5 K stratosphere	2 K troposphere 5 K stratosphere	Temperature	1.5 K 0-20km 2.0 K 20-30km 5.0 K 30km -	
Solar line shift	0.005 cm <sup>-1</sup>	0.005 cm <sup>-1</sup>	Line intensity		20.0%
Solar line strength	0.1 %	0.1 %	Line T broadening		10.0%
Solar zenith angle	0.01 Degrees	0.01 Degrees	Line P broadening		10.0%
Phase	0.001 Rad	0.001 Rad	Interfering species		HITRAN2012: varies
Zero level	0.01	0.01	Instrumental Line Shape (ILS)		10%
Background curvature		0.001 cm <sup>-2</sup>	Influence a priori profiles	Calculated	
Field of view		0.001	Solar Zenith Angle (SZA)	0.2 degrees	
Line intensity		20.0%			
Line T broadening		10.0%			

Line P broadening		10.0%			
Interfering species	HITRAN2012: varies				

**Table 4** Mean random and systematic errors for each of the individual NH<sub>3</sub> retrieval parameters. The table is split into two sections to cover both the error calculation using SFIT4 (Bremen, Lauder, Reunion) and SFIT2 (Jungfraujoch). At the bottom the errors are summarized into total mean errors for each of the stations.

Station	Bremen		Lauder		Reunion		Jungfraujoch		
	Mean Random Error (%)	Mean Systematic Error (%)	Mean Random Error (%)	Mean Systematic Error (%)	Mean Random Error (%)	Mean Systematic Error (%)	Parameter	Mean Random Error (%)	Mean Systematic Error (%)
Temperature	4.9	4.9	3.6	3.6	2.7	2.9	Temperature	15.2	
Solar zenith angle	1.6	1.6					Solar zenith angle	1.9	
Phase	1.0	1.0	1.1	1.1			Instrumental lineshape		1.4
Zero level	5.0	5.0	6.8	6.8					
Measurement noise	4.5		8.4		10.9		Measurement noise	18.2	
Interfering Species	1.3		2.4		0.9	8.7 (H <sub>2</sub> O line pressure broadening)	Interfering species		1.4
Retrieval parameters	0.1		0.1				Model parameters	1.4	
Background curvature		1.1		1.2		0.3	Forward model		1.0
Smoothing error		2.8		8.1	10.3		Smoothing	5.4	
Spectroscopy		21.0		22.7		17.8	Spectroscopy		20.1
							NH <sub>3</sub> a priori		6.1
							Influence a priori profiles (H <sub>2</sub> O & HDO)	6.6	
Subtotal error	9.1	23.5	12.0	27.0	15.3	20.0	Subtotal error	25.3	23.1
Total error	25.8		30.2		25.2		Total	34.2	

**Table 5** Statistics of the NH<sub>3</sub> columns. (Nr: number of data points, DOFS: Degree of Freedom for Signal, Mean  $\pm$  the error of the mean, RMS: Root Mean Square). Total columns are given in 1e15 molecules NH<sub>3</sub> cm<sup>-2</sup>.

Station	Nr	Mean DOFS	Mean (molecules x 1e15)	Median (molecules x 1e15)	RMS (molecules x 1e15)
Bremen	554	1.9	13.75 $\pm$ 4.24	9.51	20.22
Lauder	2412	1.4	4.17 $\pm$ 1.40	2.85	5.95
Reunion	1262	1.0	0.80 $\pm$ 0.54	0.56	1.14
Jungfraujoch	2702	1.0	0.18 $\pm$ 0.07	0.15	0.22

681

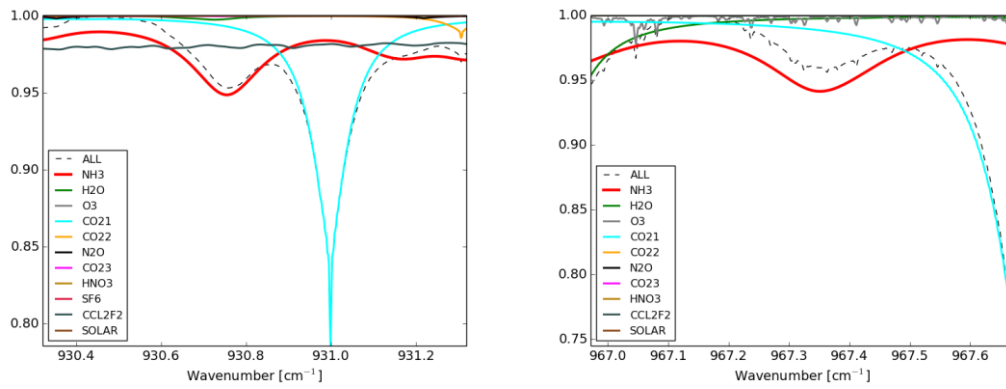
682

683

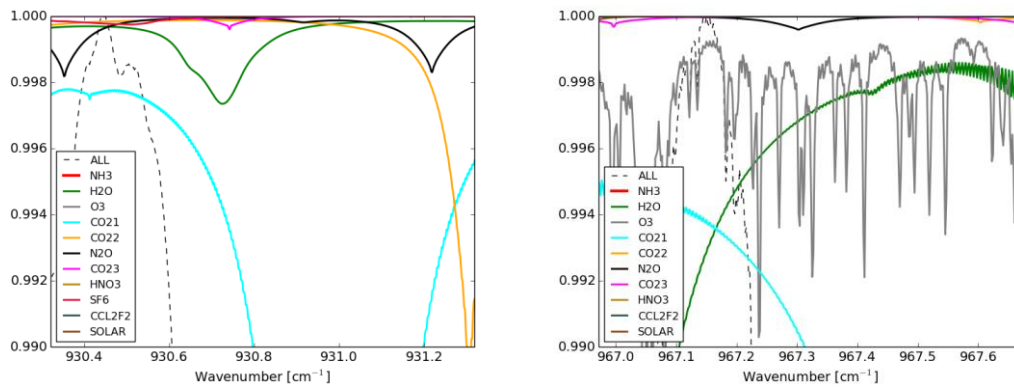
684

685 **Figures**

686

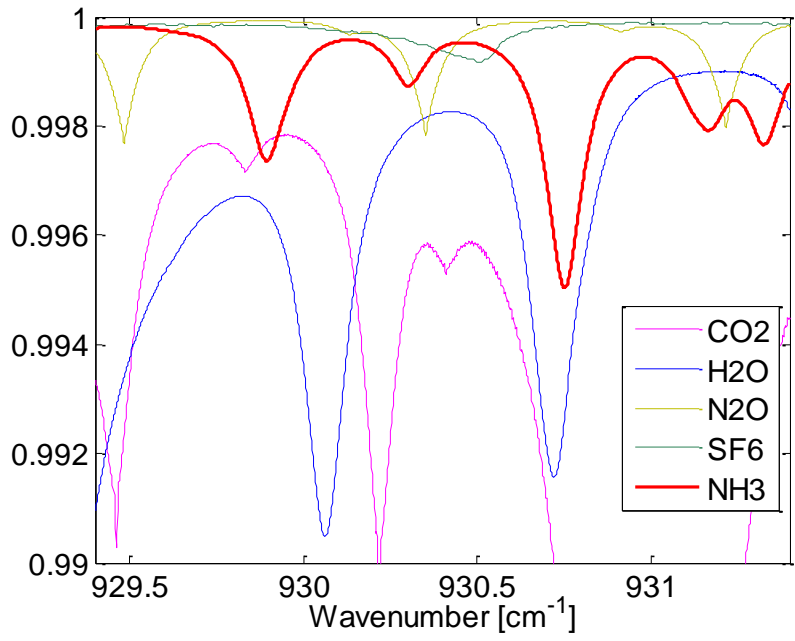


687

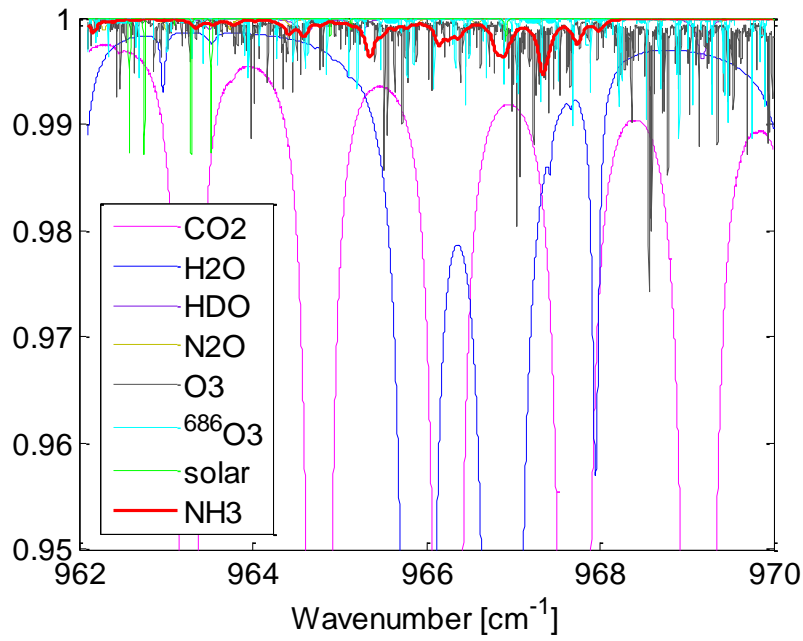


688 Figure 1 Calculated spectrum for both spectral windows measured with the 125HR in Bremen on the 19th of  
689 April 2010 at 09:59 (UTC) corresponding to a total column of 18.83e15 molecules cm<sup>-2</sup>. The top two panels  
690 show the individual contributions of the different species in the first (MW1) and second (MW2) spectral  
691 windows. The second row show the same calculated spectra but now with the y-axis scaled to show the minor  
692 interfering species.

693



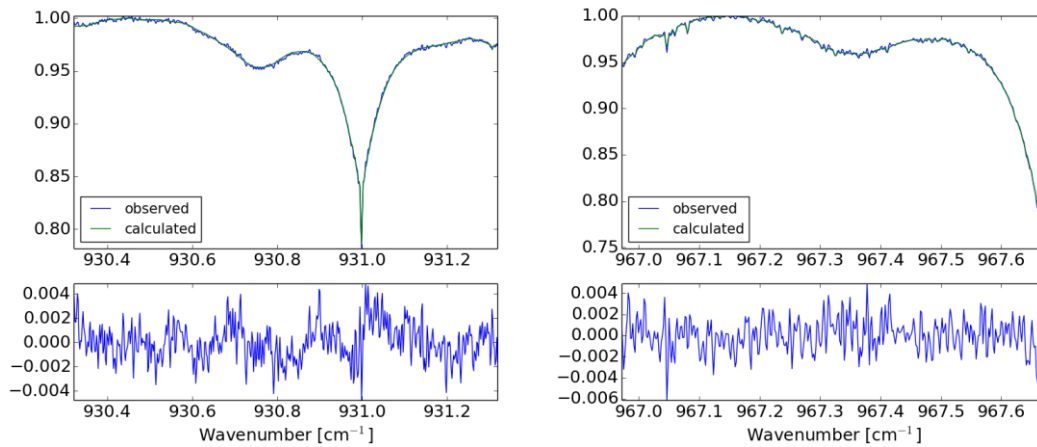
694



695

Figure 2 Example of a synthetic atmospheric spectrum for both spectral windows at Reunion Island, computed for the 5<sup>th</sup> June 2011 and a total column of 1.07E15 molecules cm<sup>-2</sup>. The top panel shows the individual contributions of the main species in the first spectral window. The bottom panel shows the second spectral window.

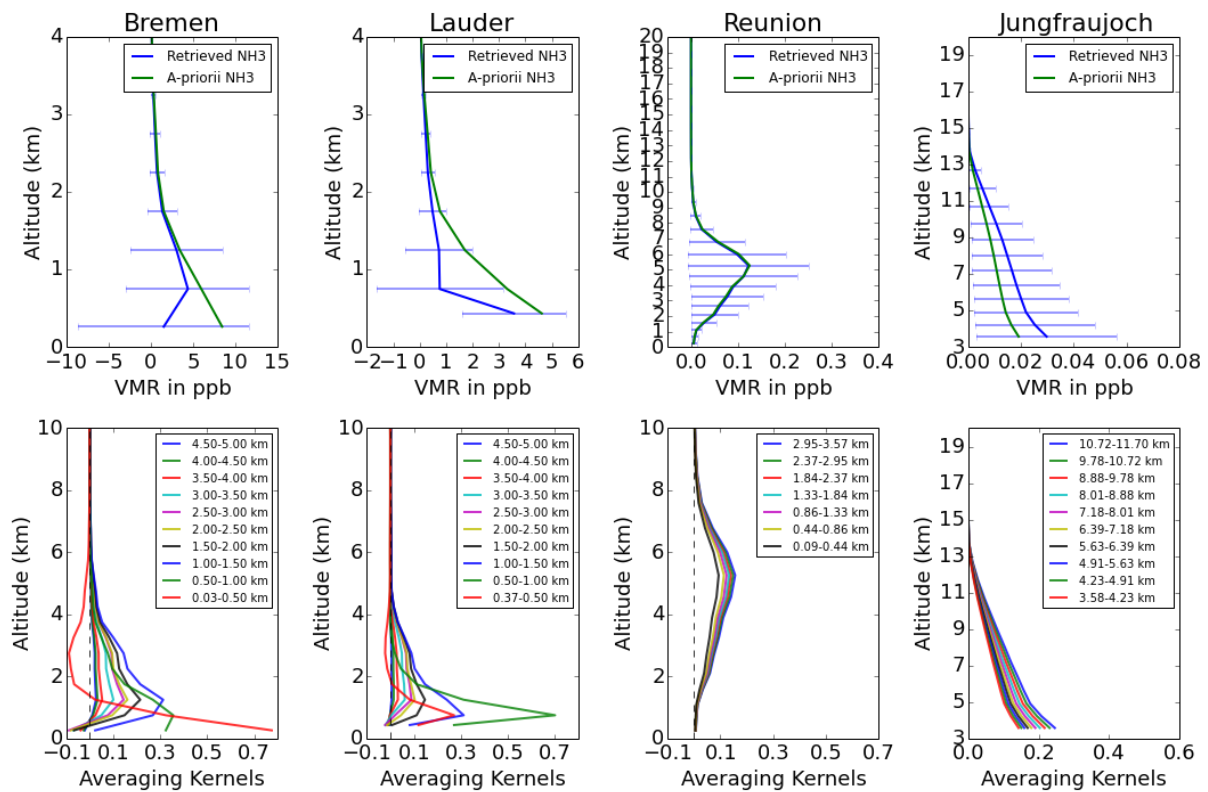
696



697

698 Figure 3 Measured and calculated spectrum for both spectral windows measured with the 125HR in Bremen on  
 699 the 19th of April 2010 at 09:59 (UTC) corresponding to a total column of  $18.83 \times 10^{15}$  molecules  $\text{NH}_3 \text{ cm}^{-2}$ . The top  
 700 two panels show the observed (blue line) and calculated (green line) spectra for MW1 (left) and MW2 (right). The  
 701 bottom two figures show the residuals of the fits in both spectral windows.

702



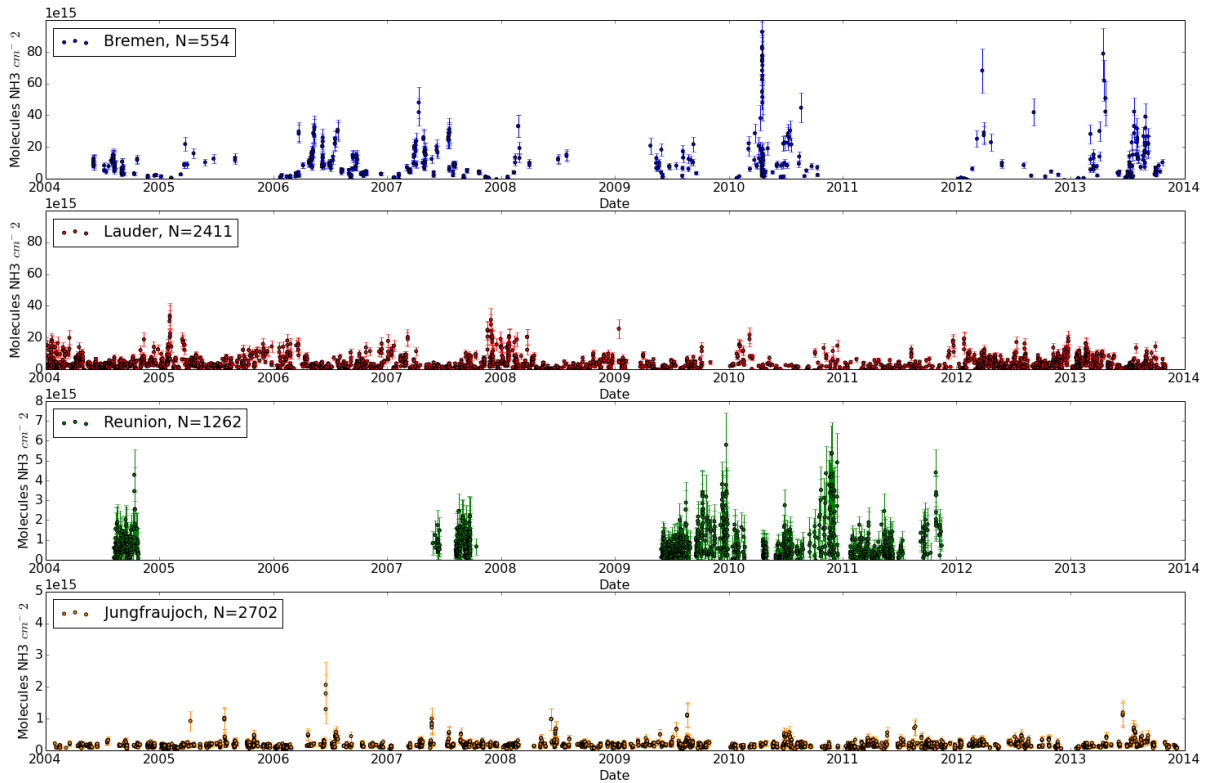
703

704 Figure 4 Top panels: the retrieved  $\text{NH}_3$  profile (blue) and the a-priori profile (green) in order from left to right:  
 705 Bremen (Left), Lauder (Left middle), Reunion island (right middle) and Jungfrauoch (right). Horizontal lines  
 706 indicate the standard deviation in all observations for each layer. Bottom panels: the normalized averaging kernel  
 707 for each of the stations.

708

709

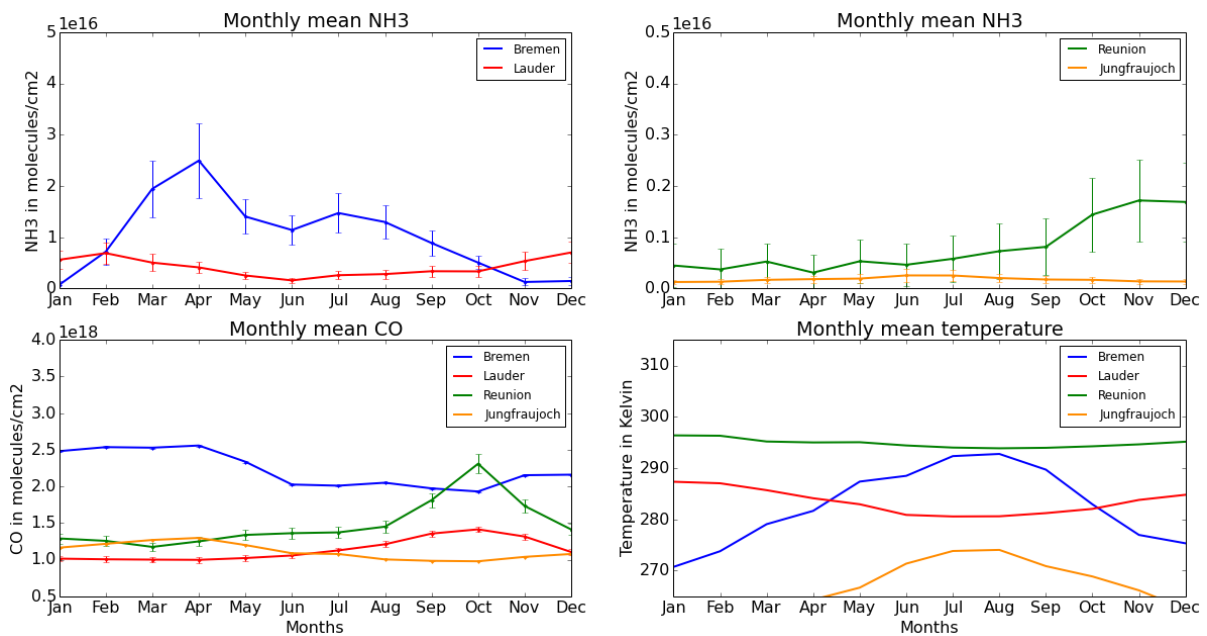
710



711

712 Figure 5 Time series of retrieved NH<sub>3</sub> columns (in molecules NH<sub>3</sub> cm<sup>-2</sup>). From top to bottom the figure shows  
713 the Bremen (blue), Lauder (red), Reunion (green) and Jungfraujoch (yellow) total columns. The bars reflect the  
714 errors on the individual observations.

715



716

Figure 6 2004-2013 monthly averaged columns for NH<sub>3</sub>, CO and temperature. The top two panels show the  
monthly NH<sub>3</sub> column concentrations (molecules NH<sub>3</sub> cm<sup>-2</sup>) for each of the four stations. Vertical lines indicate the

mean monthly error. The bottom two panels show additional column concentrations of CO (bottom, left) and temperature (bottom, right).